Available online at www.sciencedirect.com

ScienceDirect

Geochimica et Cosmochimica Acta 163 (2015) 126–139

Geochimica et Cosmochimica Acta

www.elsevier.com/locate/gca

Equilibrium magnesium isotope fractionation between aqueous Mg^{2+} and carbonate minerals: Insights from path integral molecular dynamics

Carlos Pinilla [a,b,c,*], Marc Blanchard [c], Etienne Balan [c], Suresh K. Natarajan [d], Rodolphe Vuilleumier [d], Francesco Mauri [c]

[a] *Earth Sciences Department, University College London, Gower Street, London WC1E 6BT, United Kingdom*
[b] *Departamento de Física, Universidad del Norte, km 5 Via Puerto Colombia, Barranquilla, Colombia*
[c] *Institut de Minéralogie, de Physique des Matériaux et de Cosmochimie (IMPMC), Sorbonne Universités – UPMC Univ Paris 06, UMR CNRS 7590, Muséum National d'Histoire Naturelle, IRD UMR 206, 4 Place Jussieu, 75005 Paris, France*
[d] *Ecole Normale Supérieure, Département de Chimie, UMR CNRS-ENS-UPMC No. 8640, 24 Rue Lhomond, F-75231 Paris Cedex 05, France*

Received 27 December 2014; accepted in revised form 3 April 2015; available online 18 April 2015

Abstract

The theoretical determination of the isotopic fractionation between an aqueous solution and a mineral is of utmost importance in Earth sciences. While for crystals, it is well established that equilibrium isotopic fractionation factors can be calculated using a statistical thermodynamic approach based on the vibrational properties, several theoretical methods are currently used to model ions in aqueous solution. In this work, we present a systematic study to determine the reduced partition function ratio (β-factor) of aqueous Mg^{2+} using several levels of theory within the simulations. In particular, using an empirical force field, we compare and discuss the performance of the exact results obtained from path integral molecular dynamics (PIMD) simulations, with respect to the more traditional methods based on vibrational properties and the cluster approximation. The results show the importance of including configurational disorder for the estimation of the equilibrium isotope fractionation factor. We also show that using the vibrational frequencies computed from snapshots taken from equilibrated classical molecular dynamics represents a good approximation for the study of aqueous ions.

Based on these conclusions, the β-factor of aqueous Mg^{2+} have been estimated from a Car–Parrinello molecular dynamics (CPMD) simulation with an ab initio force field, and combined with the β-factors of carbonate minerals (magnesite, dolomite, calcite and aragonite). Mg β-factor of Mg-bearing aragonite, calculated here for the first time, displays a lower value than the three other carbonate minerals. This is explained by a strong distortion of the cationic site leading to a decrease of the coordination number during Ca–Mg substitution. Overall, the equilibrium magnesium isotope fractionation factors between aqueous Mg^{2+} and carbonate minerals that derive from this methodological study support the previous theoretical results obtained from embedded cluster models.

* Corresponding author at: Departamento de Fisica, Universidad del Norte, km 5 via Puerto Colombia, Barranquilla, Colombia. Tel: +5753509509x4832.
E-mail address: c.pinilla@ucl.ac.uk (C. Pinilla).

http://dx.doi.org/10.1016/j.gca.2015.04.008
0016-7037/

1. INTRODUCTION

Marine biogenic carbonates, with their traditional C and O isotopes as well as with their cationic substitutions, represent valuable geological archives that are often used for accessing the physical and chemical conditions prevailing at the time of mineral precipitation. In this context, magnesium isotopes provide additional information in order to reconstruct paleoenvironments (Anbar and Rouxel, 2007; Johnson et al., 2008; Wu et al., 2012). However many processes may influence Mg isotope fractionation and thus complicate the interpretation of the observed variability of natural data: temperature, precipitation rate, aqueous Mg concentration, pH and the nature of precipitated mineral phases (see *e.g.* Saenger and Wang, 2014 for a review). Paleoenvironmental reconstructions necessitate a preliminary thorough understanding of Mg isotope fractionations occurring between the Mg-bearing carbonate minerals and aqueous solution where Mg exists as hexaaquo complex, *i.e.* $Mg(H_2O)_6^{2+}$. This is the aim of the few experimental studies that have investigated the Mg isotope fractionation between abiogenic carbonate minerals (calcite, aragonite, magnesite) and aqueous solution (Immenhauser et al., 2010; Li et al., 2012; Pearce et al., 2012; Saulnier et al., 2012; Mavromatis et al., 2013; Wang et al., 2013). These experimental works have been complemented by theoretical studies (Black et al., 2007; Rustad et al., 2010a,b; Schauble, 2011). Rustad et al. (2010b) used high-level quantum chemistry calculations performed on molecular clusters to study the fractionation of Mg isotopes between carbonate minerals (calcite, magnesite, dolomite) and aqueous magnesium. Schauble (2011) used instead density functional theory calculations with periodic boundary conditions to determine the isotopic fractionation between several minerals (including magnesite and dolomite) and several salts containing the $Mg(H_2O)_6^{2+}$ solvation complex. Significant discrepancies are reported between experimental data, between theoretical data, and when experimental and theoretical data are confronted together (*e.g.* Pearce et al., 2012; Wang et al., 2013; Saenger and Wang, 2014).

In almost all these previous theoretical studies the mass dependence of the isotope fractionation is dealt with through the calculation of the vibrational properties of the system of interest (Bigeleisen and Mayer, 1947; Richet et al., 1977). For crystals, the calculation of these vibrational properties is well established and many examples in the literature show that the calculated infrared and Raman frequencies, vibrational density of states and phonon dispersion curves are reliable. The equilibrium isotope fractionation factor can thus be computed using methods based on an empirical description of the inter-atomic interactions (Patel et al., 1991) or more accurately through first-principles calculations (Schauble et al., 2006; Méheut et al., 2007, 2009, 2010; Blanchard et al., 2009; Jahn and Wunder, 2009; Li et al., 2009; Rustad et al., 2010b; Javoy et al., 2012; Huang et al., 2013, 2014; Sherman, 2013; Balan et al., 2014).

Calculation of the vibrational properties of liquids and solvated elements represents a bigger challenge, which must be overcome to produce reliable solid–liquid isotopic fractionation factors. The liquid phase is usually treated by means of the cluster approximation (Liu and Tossell, 2005; Rustad et al., 2010a,b; Fujii et al., 2013; Sherman, 2013) where the species of interest is surrounded by an explicit or implicit solvation shell and this whole structure is optimised at $T = 0$ K by minimizing the forces acting on the atoms. This method has the disadvantage of neglecting the constant exchange of particles within the solvation shells and other effects of bond forming, temperature- and pressure-induced structural modifications that are thought to be important for the calculation of the isotope fractionation (Bigeleisen and Mayer, 1947; Jahn and Wunder, 2009). Another approach consists in making use of ab initio molecular dynamics and periodic boundary conditions. Using this approach, Rustad and Bylaska (2007) estimated the velocities correlation of the liquid phase and through its Fourier transform found the vibrational density of states to predict the fractionation factor of $^{11}B/^{10}B$ in an aqueous solution. From the same type of calculations Kowalski and Jahn (2011) and Kowalski et al. (2013) estimated the fractionation factors between aqueous solutions and solid minerals at high temperature by calculating the force constants acting on the fractionating element only, an approximation proposed by Bigeleisen and Mayer (1947).

In a recent study, we have discussed the performance and accuracy of these different theoretical approaches used to estimate equilibrium isotope fractionation factors in homogeneous liquid systems (Pinilla et al., 2014). Furthermore, we have used the fact that for a given potential, the fractionation factor can be exactly associated to quantum kinetic energy differences between two different isotopologues (Polyakov and Mineev, 2000; Morrone and Car, 2008; Ramirez and Herrero, 2011) and have performed path integral molecular dynamics simulations (PIMD). These methods were applied to the estimate of the D/H and $^{18}O/^{16}O$ equilibrium fractionation factors between liquid, solid and vapour phases of water (Pinilla et al., 2014). The advantage of PIMD lies on the inclusion of the effects of quantum nuclear delocalisation, and on taking into account anharmonic effects, system size and long-range effects when calculating thermodynamic quantities.

In the present work, we extend this previous study to the case of equilibrium between aqueous solutions and solids. We concentrate our efforts on the study of the accurate estimate of the equilibrium magnesium isotope fractionation between aqueous Mg^{2+} and carbonate minerals (magnesite, dolomite, calcite and aragonite). In particular, for the liquid phase, we compare and discuss the performance of the exact PIMD results with respect to the more traditional methods based on vibrational properties and the cluster approximation.

2. METHODS

2.1. The equilibrium isotope fractionation factor from vibrational properties

The equilibrium isotope fractionation factor (α factor) of an element displaying two isotopic forms Y and Y^* between two phases a and b is related to the ratio of the isotope concentration ratios:

$$\alpha(a,b,Y) = \frac{(n_{Y^*}/n_Y)_a}{(n_{Y^*}/n_Y)_b}, \quad (1)$$

where $n_{Y,a}$ is the mole fraction of isotopes Y in phase a. The equilibrium fractionation factor between two phases can be related to the reduced partition function ratio $\beta(a,Y)$ of each phase: $\ln(\alpha(a,b,Y)) = \ln(\beta(a,Y)) - \ln(\beta(b,Y))$. Isotopic fractionation factors are usually reported as $10^3\ln(\alpha(a,b,Y))$ in permil (‰). The reduced partition function ratio $\beta(a,Y)$ describes the isotopic fractionation properties of a given phase normalized to the properties of a classically-behaving system. The $\beta(a,Y)$ factor is thus usually described as the equilibrium isotope fractionation factor between the phase a and an ideal gas of atoms Y as:

$$\beta(a,y) = \frac{(n_{Y^*}/n_Y)_a}{(n_{Y^*}/n_Y)_{gas}}. \quad (2)$$

It can be shown that within the harmonic approximation and using the Teller–Redlich rule for frequencies (Wilson et al., 1955) the $\beta(a,Y)$ factor of minerals in the solid phase can be written as (Méheut et al., 2007):

$$\beta(a,Y) = \left[\prod_{i=1}^{3N_{at}} \prod_{\{q\}} \frac{\nu^*_{q,i}}{\nu_{q,i}} \frac{e^{-h\nu^*_{q,i}/(2k_BT)}}{1-e^{-h\nu^*_{q,i}/(k_BT)}} \times \frac{1-e^{-h\nu_{q,i}/(k_BT)}}{e^{-h\nu_{q,i}/(2k_BT)}}\right]^{(1/N\times N_q)} \quad (3)$$

where $\nu_{q,i}$ are the frequencies of the phonons of the i-th branch with wave vector q. N_{at} is the number of atoms in the unit-cell, and N is the number of sites occupied by the Y atom in the unit-cell. T is the temperature and k_B is the Boltzmann constant. $\nu^*_{q,i}$correspond to frequencies of the phase containing the heavy isotope. The product of Eq. (3) is usually performed on a grid containing N_q q vectors to ensure full convergence.

2.2. The equilibrium isotope fractionation factor and the kinetic energy

The β factor can be expressed in terms of the kinetic energy of the isotopologues as (*e.g.* Feynman and Hibbs, 1965; Tuckerman, 2010; Pinilla et al., 2014):

$$\ln(\beta(a,Y)) = \frac{1}{k_BT}\int_m^{m^*} dm' \frac{\langle K_a(m')\rangle}{m'} - \frac{3}{2}\ln\left[\frac{m^*}{m}\right]. \quad (4)$$

The equilibrium fractionation factor in Eq. (4) can be calculated by thermodynamic integration. $\langle K_a(m')\rangle$ represents the thermodynamic average of the kinetic energy of an atom of mass m' in phase a. These averages can be calculated exactly for a given force field using PIMD methods (see Tuckerman, 2010, for a description).

Here we have used the centroid virial estimator for the calculation of the kinetic energy:

$$K_a(m) = \frac{3}{2}k_BT - \frac{1}{2P}\left\langle \sum_{k=1}^{P}(\boldsymbol{r}_i^{(k)} - \boldsymbol{r}_i^{(C)}) \cdot \frac{\partial U(\boldsymbol{r}_i^{(k)})}{\partial \boldsymbol{r}_i^{(k)}} \right\rangle_a. \quad (5)$$

where P is the total number of beads used, $\langle\rangle_a$ represents an ensemble average on phase a and $\boldsymbol{r}_i^{(k)} - \boldsymbol{r}_i^{(C)}$ is a vector from the centre of the polymer to the position of the k-th bead as depicted in Pinilla et al. (2014). Finally, $-\frac{\partial U(r_i^{(k)})}{\partial r_i^{(k)}}$ is the total force on that bead, (*i.e.* that related to the inter-atomic potential plus that arising from the harmonic coupling to other beads). The first part of Eq. (5) can be seen as the kinetic energy of a free particle whilst the second one represents the quantum confinement of a particle due to the neighbouring atoms. This last term is related to intra-molecular interactions such as atomic bonding. If the atom behaves classically then $r_i^{(k)} - r_i^{(C)} = 0$ since the polymer has only one bead ($P = 1$), and the total fractionation amounts to zero.

2.3. Computational details

We have carried out PIMD simulations within the staging approach (Tuckerman and Berne, 1993) as implemented in the PINT module of the CP2K suite of codes (Krack and Parrinello, 2004; Yujie et al., 2006). We have used a point charge polarizable and dissociable potential for water (Pinilla et al., 2012). This model has been parameterised to reproduce many of the experimental structural and dynamical properties of liquid water. This force field is fully atomistic and no constrains are applied to any of the atoms forming the water molecule allowing for full molecular dissociation if needed. The induced dipole on the O atom is estimated self-consistently at each MD step and a short-range correction to include empirically electronic distortions due to neighbouring atoms is added (Aguado and Madden, 2003; Pinilla et al., 2012). In order to describe the interaction between the water molecules and the Mg ion we have used the fitting procedure described by Tazi et al. (2012) to extend the original water force field to include the solvation of a Mg^{2+} ion. In this case, we have described the Mg–O(H_2) interaction using the Fumi-Tosi potential form given by (Fumi and Tosi, 1964):

$$U(r) = Ae^{-B\times r} - \frac{C}{r^6} - \frac{D}{r^8}$$

with A, B, C and D the fitted parameters given in Table 1. The net ionic charge on the Mg atom has been chosen to +2e.

Liquid water simulations containing a Mg^{2+} ion were performed using simulation boxes containing 32 or 64 water molecules and an uniform charge background. Calculations have been carried out within the NVT ensemble using $P = 32$ beads which was found enough to get acceptable equilibrium isotope fractionation factors (Pinilla et al., 2014). The temperature was controlled via a Nosé–Hoover chain of three thermostats (Martyna et al., 1992). Expected averages were derived in runs of 3×10^5 molecular dynamics steps. Finally, the integral in Eq. (4) has been estimated using the trapezoidal rule with 7 masses equally spaced between the masses of ^{26}Mg and ^{24}Mg. The volume of the simulation cell is fixed so that all calculations have been performed at the experimental gas–liquid coexistence densities of water (Wagner and Pruss, 2002). In addition to PIMD calculations, fractionation factors have been estimated using phonon frequencies computed from snapshots taken from equilibrated classical molecular dynamics for the liquid phase. Final reported fractionation factors have been calculated using an average on 500 snapshots

Table 1
Force field parameters for the interaction of a Mg^{2+} ion with O atoms belonging to water molecules.

	A (Hartree)	B ($Å^{-1}$)	C (Hartree * $Å^6$)	D (Hartree * $Å^8$)
Mg–O	47.95	3.50	0.001	0.001

of the liquid system at each one of the reported temperatures (from 300 K to 600 K). In this approach the atomic positions of each snapshot have not been relaxed and the subsequent imaginary frequencies have been neglected in the final calculation of the fractionation factor (see Pinilla et al. (2014), for an extended discussion on the performance of this approach). From now on we will refer to fractionation factors found using this method as the FF-MD results. Using the same setup of parameters and the same number of snapshots, we have performed zero-temperature constant-volume optimisations of the atomic positions in order to minimise the total energy. Subsequently, we have used the relaxed configurations to calculate vibrational properties and estimate the fractionation factor. Fractionation factors calculated using this last set of frequencies will be referred as the FF-RELAX results. A summary of the methods used in the present study can be found in Table 2.

For comparison, we have performed Car–Parrinello molecular dynamics (CPMD) of the solvated Mg^{2+} ion in water using the generalised gradient approximation as proposed by Perdew et al. (1996). The ionic cores were described by ultra-soft pseudopotential from the gbrv library (Garrity et al., 2014) with an energy cutoff of 35 Ry, which was found to be enough for the convergence of vibrational properties of liquid water. These CPMD calculations were performed using the CP module within QUANTUM-ESPRESSO using a timestep of 5×10^{-3} ps. and a Nosé thermostat. It is known that DFT-PBE functionals produce an over structured phase of water if calculations are performed at room temperature (Sprik et al., 1996; Silvestrelli and Parrinello, 1999; Grossman et al., 2004). In addition, Grossman et al. (2004) have shown that the selection of the fictitious electronic mass in CP is critical for the structure of water and that in fact masses above 760 a.u. produce liquids that are much less structured with a strong dependence of the liquid structure on the mass value. In the present study, calculations were performed using a fictitious electronic mass of 700 a.u., and a temperature of 400 K. With these parameters, the water structure is similar to the one seen experimentally at room temperature (Sit and Marzari, 2005). Snapshots were taken from an equilibrated 14 ps CPMD trajectory. Phonon frequencies of the un-relaxed and relaxed structures were computed from first-principles using the linear response method (Baroni et al., 2001). Calculations were done with the PWscf and PHonon modules of the QUANTUM-ESPRESSO code (Giannozzi et al., 2009). Fractionation factors calculated using these sets of frequencies will be referred as AI-MD and AI-RELAX. For minerals, we have used the same computational parameters as for the aqueous Mg^{2+}, *i.e.* same pseudopotentials, same functional. The wave-functions and the charge density were expanded in plane-waves with 60 and 300 Ry cutoffs, respectively. Simulation cells are described in Table 3. Cell parameters were fixed to the experimental values. Only atomic positions were relaxed before calculating the phonon frequencies. Note that the theoretical frequencies are sometimes corrected by applying a general or mineral-specific scaling factor (Black et al., 2007; Kowalski and Jahn, 2011; Schauble, 2011). Here no correction has been applied.

In addition to calculations using periodic systems, we have performed calculations for the $[Mg(H_2O)_6{\cdot}12(H_2O)]^{2+}$ cluster using the configuration provided by Rustad et al. (2010b) as starting point. We performed a structure optimisation and a subsequent vibrational study for this structure using classical force field and ab initio methods. In the case of the force field the geometry optimization of the charged isolated system has been performed using a large cell size (800 Å) to minimize the electrostatic interaction between equivalent images. For ab initio calculations we have optimized the structure using the Martyna–Tuckerman correction for isolated systems (Martyna and Tuckerman, 1999). Vibrational properties have been estimated using the frozen phonon approximation as implemented in the code PHONOPY (Togo et al., 2008). We have compared β-factors estimated using the above

Table 2
Summary of all the methods used in this work for the calculation of the isotope fractionation factors.

Method	Configurations	$10^3\ln(\beta)$
FF-PIMD	Full trajectory from a 32 beads PIMD calculation performed at a given temperature	Calculated using the isotope's kinetic energy (Eq. (4)) Exact reference method including anharmonicity and quantum effects.
FF-MD or AI-MD	Snapshots taken from a classical MD trajectory – no relaxation of atomic positions to the equilibrium point performed	Calculated through vibrational properties (Eq. (3))
FF-RELAX or AI-RELAX	Snapshots taken from a classical MD trajectory – relaxation of atomic positions to the equilibrium point performed	Calculated through vibrational properties (Eq. (3))
FF-CLUSTER or AI-CLUSTER	Optimized structure for the $Mg(H_2O)_6{\cdot}[12(H_2O)]^{2+}$ cluster	Calculated through vibrational properties (Eq. (3))

Table 3
Description of the simulation cells built for carbonate minerals.

	Lattice parameters	Simulation cell	k-Points grid	q-Points grid
Magnesite $MgCO_3$ $R\bar{3}c$	Rhombohedral cell $a = 5.6760$ Å $\alpha = 48.184°$ Ross (1997)	Primitive cell 10 atoms	$3 \times 3 \times 3$ shifted	$2 \times 2 \times 2$ shifted
Dolomite $CaMg(CO_3)_2$ $R\bar{3}$	Rhombohedral cell $a = 6.0138$ Å $\alpha = 47.108°$ Ross and Reeder (1992)	Primitive cell 10 atoms	$3 \times 3 \times 3$ shifted	$2 \times 2 \times 2$ shifted
Calcite $CaCO_3$ $R\bar{3}c$	Rhombohedral cell $a = 6.3746$ Å $\alpha = 46.063°$ Markgraf and Reeder (1985)	$2 \times 2 \times 2$ supercell 80 atoms 1 Mg–Ca substitution 6.25 mol% Mg	$1 \times 1 \times 1$ shifted	$1 \times 1 \times 1$ shifted
		$4 \times 2 \times 2$ supercell 160 atoms 1 Mg–Ca substitution 3.12 mol% Mg	$1 \times 1 \times 1$ shifted	Calculation of only the force constants involving Mg
Aragonite $CaCO_3$ $Pmcn$	$a = 4.9614$ Å $b = 7.9671$ Å $c = 5.7404$ Å de Villiers (1971)	$2 \times 1 \times 2$ supercell 80 atoms 1 Mg–Ca substitution	$1 \times 1 \times 1$ shifted	$1 \times 1 \times 1$ shifted

mentioned energy cutoff (*i.e.* 35 Ry) with results using a larger cutoff of 70 Ry and have found differences smaller than 0.5‰. Results from these methods will be mentioned as FF-CLUSTER and AI-CLUSTER respectively.

3. RESULTS AND DISCUSSION

3.1. Kinetic energy of the Mg nuclei

The difference of kinetic energy for the Mg ion between values estimated using PIMD and the classical limit ($3k_BT/2$) can be found in Fig. 1. There is an increase of kinetic energy with temperature, while changing the mass from ^{24}Mg to ^{26}Mg leads to a decrease of 0.2% of the kinetic energy. In the case of ^{24}Mg the quantum contribution to the kinetic energy is less than 0.6 kJ/mol at 300 K and decreases with temperature. The difference in quantum and classical Mg kinetic energy is thus significantly smaller than that previously observed for lighter atoms, such as hydrogen (Pinilla et al., 2014). The inset of Fig. 1 shows the difference of kinetic energy for different temperatures and for different selected masses between the mass of ^{24}Mg and that of ^{26}Mg. The functional dependence of kinetic energy on the mass is less than 0.1 kJ/mol. Although in this work we have used seven different masses between ^{24}Mg and ^{26}Mg, this result suggests that a lesser number of intermediate masses will yield similar results when performing the integral of Eq. (4).

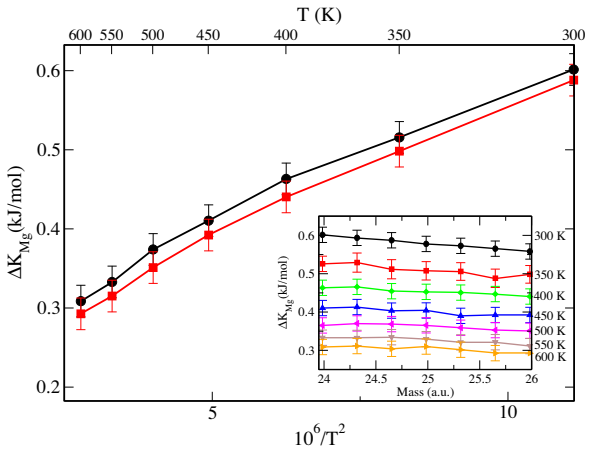

Fig. 1. Calculated Mg contribution to the kinetic energy (K_{Mg}) in aqueous solution as a function of temperature. Black circles and red squares correspond to the estimated kinetic energy difference (ΔK_{Mg}) between values from PIMD and the classical limit ($3k_BT/2$) using the masses of ^{24}Mg and ^{26}Mg, respectively. The inset shows ΔK_{Mg} for different values of mass between ^{24}Mg and ^{26}Mg and different temperatures.

3.2. Mg reduced partition function ratios (β-factors) in aqueous solution

We have calculated $^{26}Mg/^{24}Mg$ reduced partition function ratios (β-factors) of aqueous Mg from vibrational properties using Eq. (3) and from PIMD through Eq. (4). In the case of FF-MD and FF-RELAX methods we note only a small difference in the reduced partition function (less than 1‰) and these curves practically overlap the PIMD results (Fig. 2a), indicating that anharmonicity and nuclear quantum effects have a small contribution in the $^{26}Mg/^{24}Mg$ β-factor, which is in line with the small difference in kinetic energy between quantum and classical values, as discussed earlier. This also means that the MD or RELAX methods are good approximations for estimating

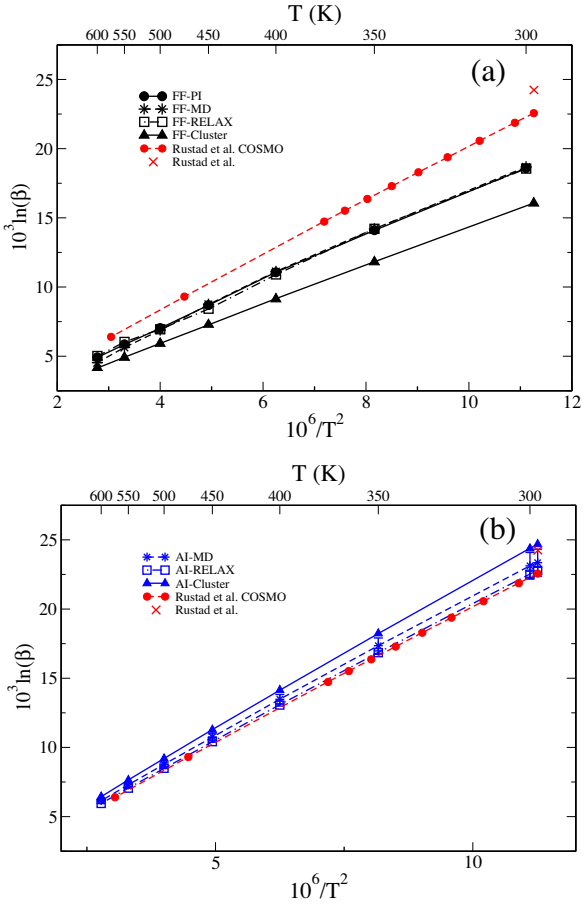

Fig. 2. $^{26}Mg/^{24}Mg$ β-factor in aqueous solution as estimated (a) from FF-PIMD (black circles), FF-MD (black stars) and FF-RELAX (black squares) methods using a supercell containing 32 water molecules. Black triangles correspond to values found using relaxed cluster structures and the classical force field as described in the text (FF-CLUSTER). (b) Using ab initio methods, blue-stars and blue-squares correspond to periodic AI-MD and AI-RELAX calculations using a 32 water molecules supercell. Blue-triangles are results using similar cluster structures (AI-CLUSTER). Red circles and crosses correspond to values reported by Rustad et al. (2010b) with and without a representation for long-range effects, respectively. Error bars for AI-MD and AI-RELAX are displayed. Error bars for other methods are found to be less than 2 ‰ and have been omitted. (For interpretation of the references to colour in this figure legend, the reader is referred to the web version of this article.)

the Mg isotope fractionation as a function of temperature. We have also performed a series of calculation using 64 water molecules to check for system size effects. We observe that the difference of β-factor values estimated from 32 and 64 molecules is of the same order of magnitude as the difference between FF-MD and FF-RELAX. This suggests that a 32 water molecules system is suitable for estimating partition function ratios in this system.

Recently, Rustad et al. (2010b) have performed accurate quantum chemistry calculations using clusters containing a solvated Mg ion in order to estimate β-factors of $^{26}Mg/^{24}Mg$ in aqueous solutions. In comparison, our calculations give lower reduced partition function ratios (Fig. 2a), which hints on the quality of the empirical force field and on the possible contribution of long-range effects to the β-factor. Rustad et al. (2010b) have discussed the importance of long-range effects by performing calculations using the 18 water molecules cluster combined with the continuous solvent model COSMO (Tomasi et al., 2005) and by comparing the results to calculations using a 32 water molecules cluster. They found that the β-factors are larger by about 2‰ at 298 K in the case of the isolated cluster than when long-range effects are taken into account. To further explore these effects, we have used the relaxed configuration for the $Mg(H_2O)_{18}$ cluster reported by Rustad et al. (2010b) to estimate $^{26}Mg/^{24}Mg$ β-factors using our force-field model (Fig. 2a). At 300 K, the β-factors estimated from cluster configurations are 2.5‰ lower than values from periodic methods such as FF-PI, FF-MD and FF-RELAX using the same force field. The differences between the cluster model and the extended system, treated with the empirical force-field, are thus of similar magnitude but in the opposite direction as those observed by Rustad et al. (2010b).

Given this difference in trend between force field calculations and those from Rustad et al. (2010b), we computed the $^{26}Mg/^{24}Mg$ β-factor of the above mentioned cluster at an ab initio (DFT-PBE) theoretical level (AI-CLUSTER). The obtained value agrees well with that reported by Rustad et al. (2010b) at 298 K using the BP86 functional and a 6-311++G(2d,2p) basis set (Fig. 2b). Fig. 2b also contains the AI-RELAX and AI-MD average β-factors as estimated using eleven snapshots from a CPMD trajectory (Fig. 4). Snapshots have been taken approximately each 0.8 ps from the last 8 ps of the trajectory. Consistent with the trend reported by Rustad et al. (2010b), we see that, in the ab initio case, the periodicity has the effect to lower down the β-factor by 1.2‰ or 1.8‰ at 300 K, considering either AI-MD or AI-RELAX (Fig. 2b).

3.3. Molecular environment of Mg ions in solution: classical force field versus ab initio model

Fig. 3 contains the O–Mg and H–Mg radial distribution function (RDF) for an Mg ion in liquid water estimated using the FF-PI, FF-MD (at $T = 300$ K) and AI-MD (at $T = 400$ K) approaches. In the case of O–Mg (H–Mg), the first peak of the RDF is shifted to longer distances by ~0.1 Å (0.05 Å) for force field based calculations when compared with AI-MD results. In addition, the RDFs show that the inclusion of nuclear quantum effects in FF-PI leads to less structured RDFs than those corresponding to classical FF-MD. This effect is especially larger in the case of H where the quantum delocalization of the proton is stronger than in the classical case for the same temperature, as indicated in the Mg–H RDF of Fig. 3b.

In order to investigate further the discrepancy between classical force field and ab initio results, we have estimated the mean Mg–O distance for the 18 water molecules cluster after relaxation (Table 4). The mean Mg–O distance is ~3% larger from the classical force field calculations than using ab initio methods. Mg–O distance using the PBE functional

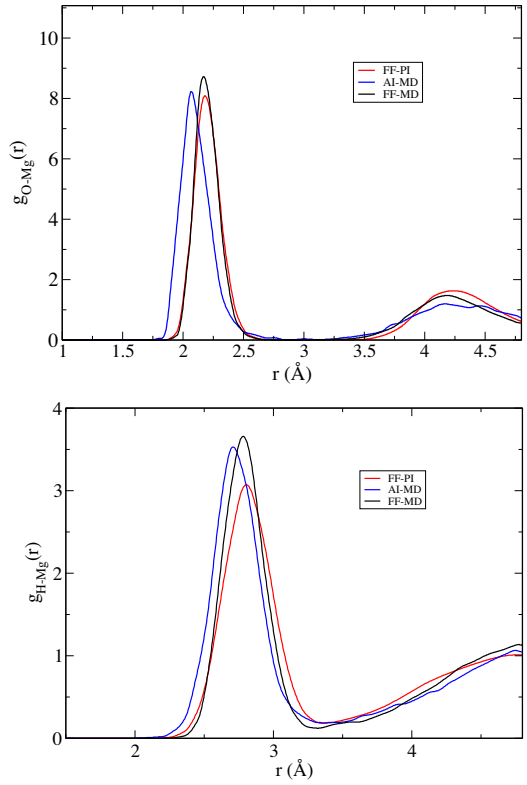

Fig. 3. O–Mg (top) and H–Mg (bottom) radial distribution function estimated using FF-PI (red), AI-MD (blue) and FF-MD (black) methods. (For interpretation of the references to colour in this figure legend, the reader is referred to the web version of this article.)

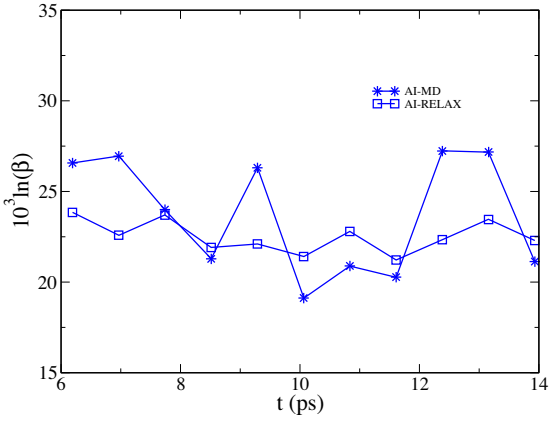

Fig. 4. $^{26}Mg/^{24}Mg$ β-factors at 300 K using 11 snapshots taken from a 14 ps CPMD run. β-Factors are estimated using the AI-MD (blue stars) and AI-RELAX (blue squares) methods. (For interpretation of the references to colour in this figure legend, the reader is referred to the web version of this article.)

(*i.e.* 2.09 Å, this study) and the BP86 functional (*i.e.* 2.11 Å, Rustad et al., 2010b) are in good agreement. The mean Mg–O bond length decreases from the cluster to the periodic description of the system when the classical force field is used, whereas the mean Mg–O bond lengths increases in ab initio methods. Since smaller bond lengths lead to higher vibrational frequencies and subsequently to larger β-factors, we believe that this contrasted structural behaviour explains the opposite trend observed in Fig. 2, *i.e.* "cluster" β-factors are smaller than "periodic" β-factors with force field methods while "cluster" β-factors are slightly larger than "periodic" β-factors with ab initio methods. Overall, our results suggest an inverse correlation between the Mg–O distance and the average value of β-factors. To investigate further the consequences of a longer/shorter Mg–O distance, we have estimated the vibrational frequencies of the $[Mg(H_2O)_6]^{+2}$ complex using the force field and ab initio approaches. Table 5 contains only the frequencies corresponding to Mg–O stretching (ν_4, ν_5, ν_6) and O–Mg–O deformation (ν_1, ν_2, ν_3) modes. As expected from the Mg–O distances, we see that force field based frequencies are lower than those from ab initio calculations; the later showing a better agreement with experimental results by Mink et al. (2003). Nevertheless, it is important to stress that this force field has been developed using as a reference a solvated Mg ion in a periodic system (containing 32 water molecules). Although we expect a high level of performance in the modelling of the structural and dynamical properties of periodic calculations, its application to isolated clusters could lead to small structural changes, of relevance when determining isotopic fractionation factors.

Table 4
Mean Mg–O distance (Å) for the aqueous Mg^{2+} as estimated from different approaches.

	d_{Mg-O}
AI-RELAX	2.13 ± 0.6
AI-MD	2.12 ± 0.8
FF-RELAX	2.16 ± 0.5
FF-PIMD	2.18 ± 0.9
FF-MD	2.18 ± 0.9
FF-CLUSTER	2.20 ± 0.1
AI-CLUSTER	2.09 ± 0.1

3.4. Temperature extrapolation

The temperature dependence for AI-MD and AI-RELAX has been determined using Eq. (3) from a CPMD calculation performed at 400 K (Fig. 2b). The procedure of using a set of vibrational properties obtained for a system at a given temperature and extrapolating the functional behaviour of β to other temperatures is a widely used approximation that can be prone to errors. Here we assess the validity of such procedure by comparing the results obtained from the FF-MD to the one obtained using the extrapolation procedure through Eq. (3) where the set of frequencies have been taken only from snapshots of a MD run performed at $T = 400$ K (Fig. 5). The extrapolation represents a good approximation, especially at low temperatures. However, the extrapolation to high temperatures does not give exactly the right asymptotic behaviour related to the sharp change in density occurring at the coexistence of liquid/vapour water. This leads to discrepancies of 0.5‰ at 600 K.

Table 5
Estimated frequencies for the $[Mg(H_2O)_6]^2$ complex (cm^{-1}).

	ν_1	ν_2	ν_3	ν_4	ν_5	ν_6
Classical force field	69	114	140	260	310	341
DFT-PBE	92	149	210	306	386	408
Exp. (Mink et al., 2003; Kapitan et al., 2010)	133	178	216	314	365	421

3.5. Statistical error of β-factor in liquids

The dispersion of β-factors obtained from the AI-MD method is larger than that obtained from the AI-RELAX calculations (Fig. 4). Given the relatively short length of the ab initio trajectory, we have used the trajectories obtained from the classical force field to analyze further this dispersion. An analysis using a larger number of data (500) to estimate the error on the average using the bin method as discussed in Allen and Tildesley (2001) shows that 90% of the FF-MD β-factors fall in an interval of 4‰ around the average value (*i.e.* 18.6‰ at $T = 300$ K) whereas for FF-RELAX this interval is only of 1‰. The FF-RELAX method, which implies the optimization of atomic positions to their equilibrium positions, has the effect of producing more homogeneous Mg–O distances and thus erases some of the dynamical effects still present in values obtained from the MD approach. The FF-RELAX uncertainty reported for the β-factors of Mg in the aqueous phase is of the same order as those reported for estimated Mg β-factors in minerals, usually of a few ‰.

3.6. Mg β-factors of carbonate minerals

The calculated temperature dependence of the β-factors of carbonate minerals and aqueous magnesium are shown in Fig. 6 and their polynomial fits are given in Table 6. They can be compared to previous theoretical estimates involving slightly different approaches (Table 7). Rustad et al. (2010b) employed embedded cluster models while Schauble (2011) used periodic systems as in the present study, but the mineral structures were fully optimized (atomic positions and lattice parameters) and frequencies were corrected by applying a uniform scale factor of 1.033. Theoretical β-factors are sometimes in reasonable agreement, like for $Mg_{(aq)}$ or magnesite ($MgCO_3$), and sometimes more scattered, like for calcite ($CaCO_3$) or dolomite ($CaMg(CO_3)_2$). Nevertheless, the relative order is always the same: dolomite > magnesite > calcite, with $Mg_{(aq)}$ between dolomite and magnesite. It is noteworthy that the estimate of the $Mg_{(aq)}$ β-factor from a set of salts containing the $Mg(H_20)_6^{2+}$ complex leads to a value ~6‰ higher than the other estimates at 298 K. This sequence dolomite > magnesite > calcite is also supported by an analysis of the crystallographic environment of Mg (*i.e.* bond length, coordination number) in the minerals (Wang et al., 2013; Saenger and Wang, 2014). For these three minerals, Mg is in octahedral site. Dolomite and magnesite show similar calculated Mg–O bond length (2.086 and 2.099 Å, respectively), which are in good agreement with experimental values (2.081 and 2.101 Å, from Ross and Reeder, 1992; Ross, 1997, respectively). Consistently, these two minerals also display similar Mg β-factors (23.2‰ and 22.6‰ at 298 K, respectively).

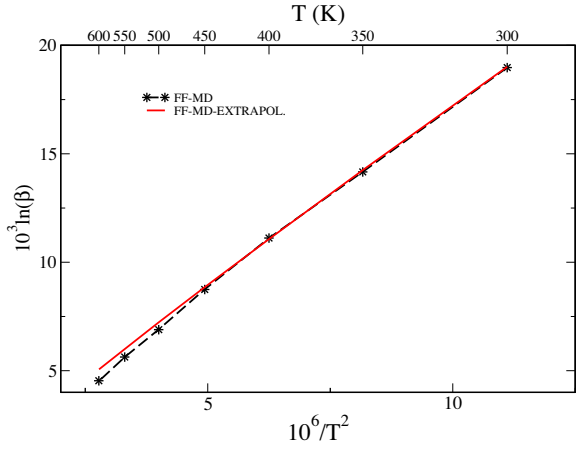

Fig. 5. $^{26}Mg/^{24}Mg$ β-factor in aqueous solution as estimated using the FF-MD method (black stars) and an extrapolation to other temperatures using MD snapshots obtained at 400 K.

Unlike magnesite ($MgCO_3$) and dolomite ($CaMg(CO_3)_2$), Mg is an impurity in calcite and aragonite. The equilibrium isotopic fractionation factors could thus depend on the Mg content, through its impact on the crystal structure. Such compositional effect was evidenced for Ca isotopes in Ca-doped orthopyroxenes, using similar theoretical methods (Feng et al., 2014; Huang et al., 2014). In order to test this assumption, we built a twice-larger simulation cell of calcite along the *a* direction ($4 \times 2 \times 2$ supercell of 160 atoms) with one Mg substitution, which corresponds to 3.125 mol% Mg. The *b* and *c* dimensions of both simulation cells are kept identical. The shortest distance between the Mg atom and its images is therefore the same (*i.e.* 9.98 Å) for both concentrations. However the atomic relaxation performed under strictly identical conditions for the two simulation cells leads to slightly different Mg–O bond lengths (2.16 Å in the $2 \times 2 \times 2$ supercell versus 2.14–2.15 Å in the $4 \times 2 \times 2$ supercell). Computing the full vibrational frequencies of such large system was not affordable. We computed instead only the force constants involving the Mg atom, *i.e.* single atom approximation (Bigeleisen and Mayer, 1947; Moynier et al., 2011). In the Mg case, this approximation slightly overestimates the β-factor by 0.8‰ below ~400 K (Fig. 6). We can however be confident in the relative values. Thus, decreasing the Mg content of calcite from 6.25 to 3.125 mol% Mg leads to an increase of the β-factor of 1.2‰ at 298 K (Table 7). By doing so, our calculated values get closer to the values

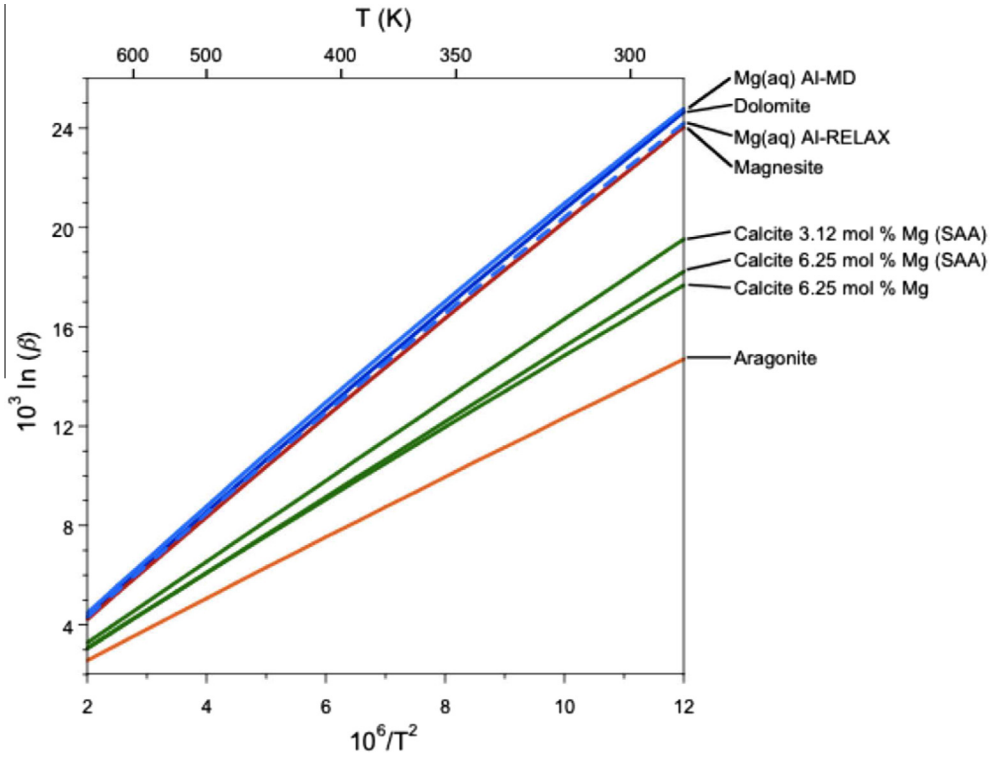

Fig. 6. Calculated $^{26}Mg/^{24}Mg$ β-factors of aqueous magnesium and carbonate minerals. All β-factors were calculated from the full vibrational frequencies except for testing the Mg concentration effect in calcite where the single atom approximation (SAA) was used, *i.e.* only the force constant acting on the Mg atom is considered for the calculation of the isotopic fractionation (Kowalski and Jahn, 2011).

Table 6
Polynomial fits of the $^{26}Mg/^{24}Mg$ fractionation factors ($10^3 \ln\beta$ and $10^3 \ln\alpha$ in ‰) based on the function $ax + bx^2 + cx^3$, with $x = 10^6/T^2$ (T in K).

	a	b	c
$Mg_{(aq)}$ AI-MD	2.2652	-1.7635×10^{-2}	7.2582×10^{-5}
$Mg_{(aq)}$ AI-RELAX	2.1872	-1.6577×10^{-2}	1.8703×10^{-4}
Dolomite	2.1882	-1.2745×10^{-2}	1.2890×10^{-4}
Magnesite	2.1370	-1.2994×10^{-2}	1.5227×10^{-4}
Calcite (6.25 mol% Mg)	1.5520	-7.8937×10^{-3}	1.0745×10^{-4}
Aragonite	1.2954	-7.1682×10^{-3}	1.0249×10^{-4}
Magnesite-$Mg_{(aq)}$	-1.2737×10^{-1}	4.4626×10^{-3}	8.8909×10^{-5}
Calcite-$Mg_{(aq)}$	-7.1146×10^{-1}	9.4480×10^{-3}	4.7365×10^{-5}
Aragonite-$Mg_{(aq)}$	-9.6950×10^{-1}	1.0404×10^{-2}	3.3191×10^{-5}
Dolomite-$Mg_{(aq)}$	-7.5743×10^{-2}	4.5981×10^{-3}	7.2001×10^{-5}

Table 7
Calculated values of $^{26}Mg/^{24}Mg$ β-factors ($10^3 \ln\beta$ in ‰) at 298 K.

	This study	Rustad et al. (2010b) BP86	Rustad et al. (2010b) B3LYP	Schauble (2011) PBE
$Mg_{(aq)}$	23.3 ± 1.0 (AI-MD) 22.8 ± 0.2 (AI-RELAX)	22.6	23.5	29.7
Dolomite	23.2	25.0	24.7	22.4
Magnesite	22.6	22.6	22.4	21.3
Calcite	18.3 (3.12 mol% Mg, SAA) 17.1 (6.25 mol% Mg, SAA) 16.6 (6.25 mol% Mg)	18.9	18.2	
Aragonite	13.8			

estimated by Rustad et al. (2010b), which corresponds to the dilute limit as modeled by the embedded cluster.

The Mg β-factor in aragonite ($CaCO_3$) is significantly lower than that determined for the other carbonates. In aragonite, the Ca coordination number is 9 instead of 6 in calcite or dolomite. The optimization of the Mg position in this large 9-fold Ca site is not straightforward. The most stable configuration found (Fig. 7) displays 5 Mg–O bonds ranging from 2.11 to 2.17 Å, with an additional longer Mg–O bond (2.64 Å). The three other oxygen atoms of the site are at a distance larger than 2.8 Å. Other configurations equivalent in energy are likely, with Mg bounds to other O atoms of the Ca site. The DFT calculations thus suggest that Mg substitution induces a large distortion of the aragonite structure, leading to the smallest Mg β-factors among the four carbonate minerals investigated. A significant relaxation of the Mg-site in aragonite is also suggested by X-ray absorption spectroscopy (Finch and Allison, 2007). Experimental data indicates that Mg in aragonite keeps a 9-fold coordination but displays relatively short Mg–O distances (2.08 Å, similar to those observed in magnesite and dolomite). Magnesium would therefore be strongly bound in aragonite, leading to a higher Mg β-factor than in magnesite and dolomite (Wang et al., 2013; Saenger and Wang, 2014). However, the extent of structural relaxation also points to the difficulty to incorporate Mg in aragonite and the occurrence in experimental samples of Mg-rich nano-domains of unknown structure is not excluded (Finch and Allison, 2007).

3.7. Equilibrium Mg isotope fractionation between carbonate minerals and aqueous solution

The equilibrium Mg isotope fractionation between carbonate minerals and aqueous solution are obtained by combining the corresponding β-factors (Fig. 8 and Table 6). Both MD and RELAX methods are acceptable approximations for estimating the Mg isotope fractionation but these two methods give slightly different β-factors (Fig. 2b). We opted here for the AI-MD results in order to include the dynamical effects of the liquid. Choosing instead the AI-RELAX results would shift all fractionation factors upward of 0.5‰ at 298 K, thus remaining within the expected error range.

Globally, our results support the predictions of Rustad et al. (2010b). The fractionation factors for magnesite-$Mg_{(aq)}$ fall in the same range as those of Rustad et al. (2010b) and are close to the measured ones by Pearce et al. (2012). For calcite-$Mg_{(aq)}$, an effect of the Mg content in the carbonate minerals is inferred from the calculation. Considering the lowest Mg concentration investigated here reconciles our results with those of Rustad et al. (2010b). The theoretical isotope fractionation (−3.0‰ at 400 K) is however larger than those experimentally determined; which are scattered from about −1.7‰ to −3.5‰ (Immenhauser et al., 2010; Li et al., 2012; Saulnier et al., 2012; Mavromatis et al., 2013). There are indications suggesting that the lowest experimental values are those approaching the equilibrium fractionation factors but isotopic equilibrium may not have been reached (Saenger and Wang, 2014).

For dolomite-$Mg_{(aq)}$, our results predict almost no isotopic fractionation at equilibrium and are therefore slightly lower than the results of Rustad et al. (2010a, 2010b). The fractionation factor inferred by Galy et al. (2002), between the dolomite of speleothems and dripwater (∼+0.33‰) would reasonably agree with the theoretical data. On the other hand, Higgins and Schrag (2010) reported larger negative fractionation factors (−2.0‰ to −2.7‰) between dolomite and the coexisting aqueous fluid in deep-sea sediments. However it must be noted that ideal dolomite is rare in modern sediments, *e.g.* Kaczmarek and Sibley (2011).

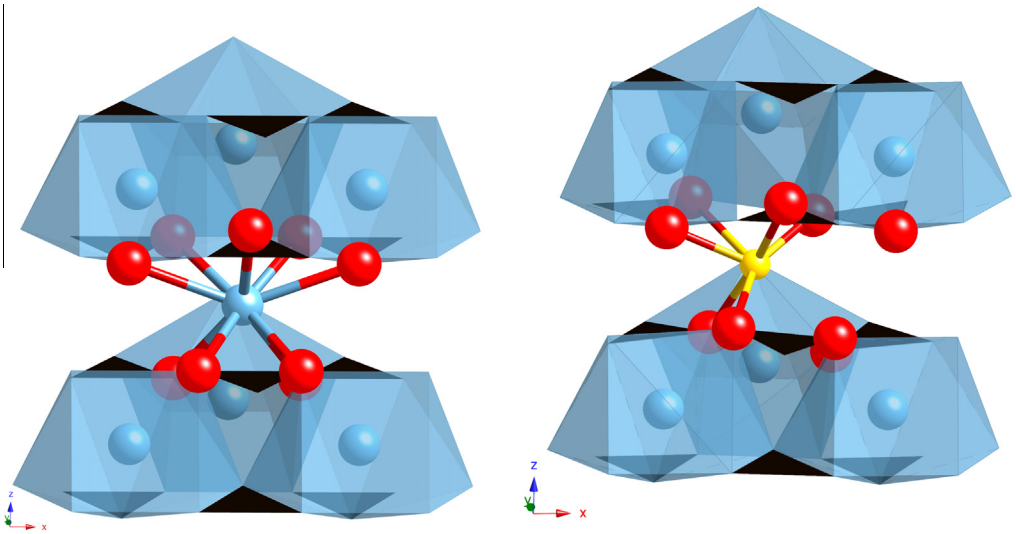

Fig. 7. Theoretical structure of pure aragonite (left) and of the most stable configuration found for Mg-bearing aragonite (right). The black triangles represent the carbonate groups. The yellow sphere is the magnesium atom while calcium atoms are in blue. The red spheres represent the oxygen atoms of the 9-fold site where the Ca–Mg substitution occurs. (For interpretation of the references to colour in this figure legend, the reader is referred to the web version of this article.)

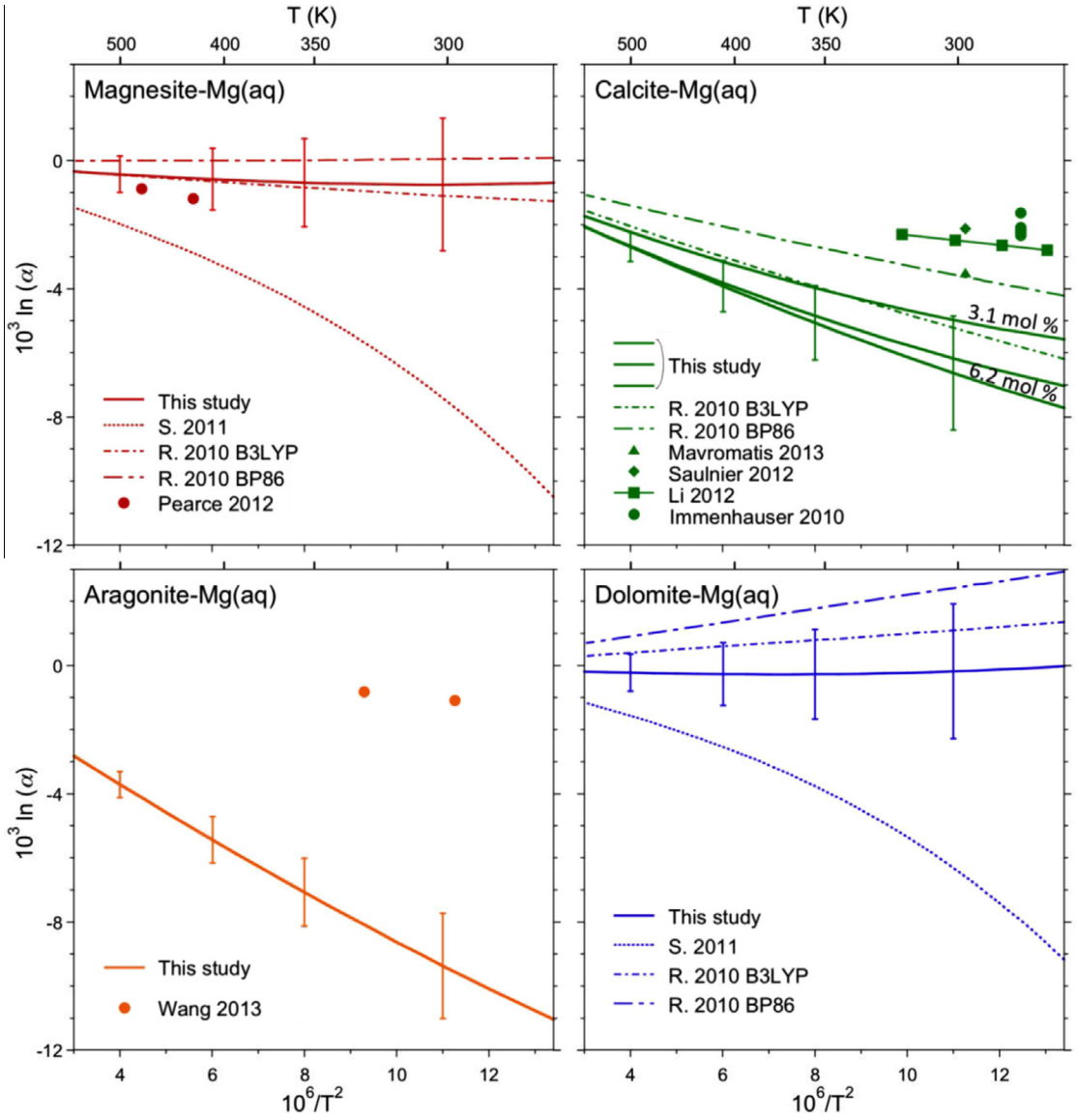

Fig. 8. Calculated and measured isotopic fractionations between carbonate minerals and aqueous magnesium. Data from this study (with AI-MD results for aqueous magnesium) are compared with theoretical data (Rustad et al., 2010b; Schauble, 2011) and experimental data (Immenhauser et al., 2010; Li et al., 2012; Pearce et al., 2012; Saulnier et al., 2012; Mavromatis et al., 2013; Wang et al., 2013). Error bars have been estimated by taking the error bars of AI-MD results and assuming a typical 5% error for the calculated vibrational frequencies of minerals (Méheut et al., 2007).

Factors such as variations in stoichiometric and cationic order may affect the isotopic composition, impacting the comparison with models of stoichiometric and well-ordered dolomite. In addition, only the hexaaquo complex, $Mg(H_20)_6^{2+}$ was modelled in the present study, whereas other Mg aqueous species may also play a role.

For aragonite-$Mg_{(aq)}$, there is a clear discrepancy between our theoretical data (−9.8‰ at 25 °C) and the experimental ones (−1.1‰) measured by Wang et al. (2013). In that case, experimental data may not represent the isotopic equilibrium between $Mg_{(aq)}$ and aragonite (Saenger and Wang, 2014) as it is not experimentally demonstrated that the Mg atoms are truly substituted for Ca in aragonite. Whereas several spectroscopic evidences support the substitution of Mg for Ca in the calcite crystal structure, it is not certain that the aragonite structure accommodates the Mg^{2+} ions, *e.g.* Mavromatis et al. (2013), Mucci and Morse (1983). Finch and Allison (2007) did not exclude the presence of Mg-rich nanodomains of an unknown phase. Moreover, Mg^{2+} ions display a strong hydration free energy compared to Ca^{2+} ions. This implies that the entrapment of hydrated Mg ions must also be considered (Mavromatis et al., 2013). Based on the assumption of a Ca–Mg substitution, the theoretical results that we report here show one possible stable configuration where the Mg substitution is accompanied by a strong local distortion of the structure (Fig. 7). Other stable configurations may exist and other incorporation mechanisms may

be more favourable at finite temperature. Thus, further investigation of the incorporation mechanism of Mg in aragonite is needed.

4. CONCLUSION

We have estimated the β-factor of aqueous Mg^{2+} using the PIMD approach in combination with a classical force field in order to include in an exact form of anharmonic and quantum effects. In addition, we have compared the performance of the PIMD results with a set of approximate approaches based on the determination of the harmonic vibrational properties of the system (namely, FF-MD, FF-RELAX and FF-CLUSTER). In agreement with the recent theoretical work of Dupuis et al. (2015) on silicon isotopes, the present results suggest that the inclusion of configurational disorder, as present in the FF-PIMD, FF-MD and FF-RELAX methods, is of relevance to obtain the right temperature dependence of the β-factor. Another important conclusion of this work is that the use of expensive PIMD to estimate β-factors can be replaced by lower cost methods (*i.e.* methods using the vibrational frequencies computed from snapshots taken from equilibrated classical molecular dynamics) that yield a similar accuracy in the case of relatively heavy ions like magnesium.

Based on these conclusions, we have estimated the β-factor of aqueous Mg^{2+} using ab initio molecular dynamics as implemented in CPMD. Results derived from the empirical force field are underestimated with respect to the ab initio results. This discrepancy highlights the importance of an accurate description of the first solvation shell of the solvated species (*i.e.* Mg–O bond lengths) in order to obtain the right trend.

Finally, we have used ab initio methods to estimate the β-factors of carbonate minerals and we have found that Mg β-factors of dolomite, magnesite and aqueous Mg^{2+} are close to each other. Calcite and then aragonite display lower Mg β-factors. The latter is explained by a strong distortion of the cationic site leading to a decrease of the coordination number during the Ca–Mg substitution. The calculated equilibrium magnesium isotope fractionation factors between aqueous Mg^{2+} and carbonate minerals are mostly consistent with previous theoretical results obtained from embedded cluster models.

ACKNOWLEDGEMENTS

This work was performed using HPC resources from GENCI-IDRIS (Grant 2014-i2014041519). This work has been supported by the French National Research Agency (ANR, project 11-JS56-001 "CrIMin"). C.P. also acknowledges partial funding from the ERC (Project No. 513209).

REFERENCES

Aguado A. and Madden P. A. (2003) Ewald summation of electronic multipole interactions upto the quadrupolar level. *J. Chem. Phys.* **119**, 7471.

Allen M. P. and Tildesley D. J. (2001) *Computer Simulation of Liquids*. Oxford University Press.

Anbar A. and Rouxel O. (2007) Metal isotopes in paleoceanography. *Annu. Rev. Earth Planet. Sci.* **35**, 717–746.

Balan E., Blanchard M., Pinilla C. and Lazzeri M. (2014) First-principles modeling of sulfate incorporation and $^{34}S/^{32}S$ isotopic fractionation in different calcium carbonates. *Chem. Geol.* **374–375**, 84–91.

Baroni S., de Gironcoli S., Corso A. D. and Giannozzi P. (2001) Phonons and related crystal properties from density functional perturbation theory. *Rev. Mod. Phys.* **73**, 515–562.

Bigeleisen J. and Mayer M. G. (1947) Calculation of equilibrium constants for isotopic exchange reactions. *J. Chem. Phys.* **15**, 261–267.

Black J. R., Yin Q.-Z., Rustad J. R. and Casey W. H. (2007) Magnesium isotopic equilibrium in chlorophylls. *J. Am. Chem Soc.* **129**, 8690–8691.

Blanchard M., Poitrasson F., Méheut M., Lazzeri M., Mauri F. and Balan E. (2009) Iron isotope fractionation between pyrite (FeS_2), hematite (Fe_2O_3) and siderite ($FeCO_3$): a first-principles density functional theory study. *Geochim. Cosmochim. Acta* **73**, 6565–6578.

Dupuis R., Benoit M., Nardin E. and Méheut M. (2015) Fractionation of silicon isotopes in liquids: the importance of configurational disorder. *Chem. Geol.* **396**, 239–254.

Feng C., Qin T., Huang S., Wu Z. and Huang F. (2014) First-principles investigations of equilibrium calcium isotope fractionation between clinopyroxene and Ca-doped orthopyroxene. *Geochim. Cosmochim. Acta* **143**, 132–142.

Feynman R. and Hibbs A. (1965) *Quantum Mechanics and Path Integrals*. McGraw-Hill, New York.

Finch A. A. and Allison N. (2007) Coordination of Sr and Mg in calcite and aragonite. *Mineral. Mag.* **71**, 539–552.

Fujii T., Mounier F., Abe M., Nemoto K. and Albarede F. (2013) Copper isotope fractionation between aqueous compounds relevant to low temperature geochemistry and biology. *Geochim. Cosmochim. Acta* **110**, 29–44.

Fumi F. G. and Tosi M. P. (1964) Ionic sizes and Born repulsive parameters in the NaCl-type alkali halides-I. *J. Phys. Chem. Solids* **25**, 31–43.

Galy A., Bar-Matthews M., Halicz L. and O'Nions R. K. (2002) Mg isotopic composition of carbonate: insight from speleothem formation. *Earth Planet. Sci. Lett.* **201**, 105–115.

Garrity K. F., Bennett J. W., Rabe K. M. and Vanderbilt D. (2014) Pseudopotentials for high-throughput DFT calculations. *Comp. Mat. Sci.* **81**, 446–452.

Giannozzi P., Baroni S., Bonini N., Calandra M., Car R., Cavazzoni C., Ceresoli D., Chiarotti G. L., Cococcioni M., Dabo I., Corso A. D., de Gironcoli S., Fabris S., Fratesi G., Gebauer R., Gerstmann U., Gougoussis C., Kokalj A., Lazzeri M., Martin-Samos L., Marzari N., Mauri F., Mazzarello R., Paolini S., Pasquarello A., Paulatto L., Sbraccia C., Scandolo S., Sclauzero G., Seitsonen A. P., Smogunov A., Umari P. and Wentzcovitch R. M. (2009) QUANTUM ESPRESSO: a modular and open-source software project for quantum simulations of materials. *J. Phys. Condens. Matter* **21**, 395502.

Grossman J. C., Schwegler E., Draeger E. W., Gygi F. and Galli G. (2004) Towards an assessment of the accuracy of density functional theory for first principles simulations of water. *J. Chem. Phys.* **120**, 300–311.

Higgins J. A. and Schrag D. P. (2010) Constraining magnesium cycling in marine sediments using magnesium isotopes. *Geochim. Cosmochim. Acta* **74**, 5039–5053.

Huang F., Chen L., Zhongqing W. and Wang W. (2013) First-principles calculations of equilibrium Mg isotope fractionations between garnet, clinopyroxene, orthopyroxene, and olivine: Implications for Mg isotope thermometry. *Earth Planet. Sci. Lett.* **367**, 61–70.

Huang F., Zhongqing W., Huang S. and Wu F. (2014) First-principles calculations of equilibrium silicon isotope fractionation among mantle minerals. *Geochim. Cosmochim. Acta* **140**, 509–520.

Immenhauser A., Buhl D., Richter D. K., Niedermayer A. D. R., Dietzel M. and Schulte U. (2010) Magnesium-isotope fractionation during low-Mg calcite precipitation in a limestone cave – field study and experiments. *Geochim. Cosmochim. Acta* **74**, 4346–4364.

Jahn S. and Wunder B. (2009) Lithium speciation in aqueous fluids at high P and T studied by ab-initio molecular dynamics and consequences for Li isotope fractionation between minerals and fluids. *Geochim. Cosmochim. Acta* **73**, 5428–5434.

Javoy M., Balan E., Méheut M., Blanchard M. and Lazzeri M. (2012) First-principles investigation of equilibrium isotopic fractionation of O- and Si-isotopes between refractory solids and gases in the solar nebula. *Earth Planet. Sci. Lett.* **319**(320), 118–127.

Johnson C. M., Beard B. L. and Roden E. E. (2008) The iron isotope fingerprints of redox and biogeochemical cycling in modern and ancient earth. *Annu. Rev. Earth Planet. Sci.* **36**, 457–493.

Kaczmarek S. E. and Sibley D. F. (2011) On the evolution of dolomite stoichiometry and cation order during high-temperature synthesis experiments: an alternative model for the geochemical evolution of natural dolomites. *Sediment. Geol.* **240**, 30–40.

Kapitan J., Dracinsky M., Kaminsky J., Benda L. and Bour P. (2010) Theoretical modeling ion imprints in the Raman scattering of water. *J. Phys. Chem. B* **114**, 3574–3582.

Kowalski P. and Jahn S. (2011) Prediction of equilibrium Li isotope fractionation between minerals and aqueous solutions at high P and T: an efficient ab-initio approach. *Geochim. Cosmochim. Acta* **75**, 6112–6123.

Kowalski P. M., Wunder B. and Jahn S. (2013) Ab-initio prediction of equilibrium boron isotope fractionation between minerals and aqueous fluids at high P and T. *Geochim. Cosmochim. Acta* **101**, 285–301.

Krack M. and Parrinello M. (2004) *High Performance Computing in Chemistry*. NIC, Jülich.

Li W., Chakraborty S., Beard B. L., Romanek C. S. and Johnson C. M. (2012) Magnesium isotope fractionation during precipitation of inorganic calcite under laboratory conditions. *Earth Planet. Sci. Lett.* **333–334**, 304–316.

Li X., Zhao H. and Yun L. (2009) Theoretical prediction for several important equilibrium Ge isotope fractionation factors and geological implications. *Earth Planet. Sci. Lett.* **287**, 1–11.

Liu Y. and Tossell J. A. (2005) Ab-initio molecular orbital calculations for Boron isotope fractionations on Boric Acids and Borates. *Geochim. Cosmochim. Acta* **69**, 3995–4006.

Markgraf S. A. and Reeder R. J. (1985) High-temperature structure refinement of calcite and magnesite. *Amer. Mineral.* **70**, 590–600.

Martyna G. J. and Tuckerman M. E. (1999) A reciprocal space based method for treating long range interactions in ab-initio and force-field-based calculations in clusters. *J. Chem. Phys.* **110**, 2810.

Martyna G. J., Klein M. L. and Tuckerman M. (1992) Nosé-Hoover Chains: the Canonical Ensemble via Continuous Dynamics. *J. Chem. Phys.* **97**, 2635–2643.

Mavromatis V., Gautier Q., Bosc O. and Schott J. (2013) Kinetics of Mg partition and Mg stable isotope fractionation during its incorporation in calcite. *Geochim. Cosmochim. Acta* **114**, 188–203.

Méheut M., Lazzeri M., Balan E. and Mauri F. (2007) Equilibrium isotopic fractionation in the kaolinite, quartz, water system: prediction from first-principles density-functional theory. *Geochim. Cosmochim. Acta* **71**, 3170–3181.

Méheut M., Lazzeri M., Balan E. and Mauri F. (2009) Structural control over equilibrium silicon and oxygen isotopic fractionation: a first-principles density-functional-theory. *Chem. Geol.* **258**, 28–37.

Méheut M., Lazzeri M., Balan E. and Mauri F. (2010) First-principles calculation of H/D isotopic fractionation between hydrous minerals and water. *Geochim. Cosmochim. Acta* **74**, 3874–3882.

Mink J., Nemeth C., Hajba L., Sandstrom M. and Goggin P. L. (2003) Infrared and Raman spectroscopic and theoretical studies of hexaaqua metal ions in aqueous solution. *J. Mol. Struct.* **661–662**, 141–151.

Morrone J. A. and Car R. (2008) Nuclear quantum effects in water. *Phys. Rev. Lett.* **101**, 017801.

Moynier F., Paniello R., Beck P., Gounelle F., Podosek F., Abarede F. and Zanda B. (2011) Nature of volatile depletion and genetic relationships in enstatite chondrites and aubrites inferred from Zn isotopes. *Geochim. Cosmochim. Acta* **75**, 297–307.

Mucci A. and Morse J. W. (1983) The incorporation of Mg^{2+} and Sr^{2+} into calcite overgrowths: influences of growth rate and solution composition. *Geochim. Cosmochim. Acta* **47**, 217–233.

Silvestrelli P. L. and Parrinello M. (1999) Structural, electronic, and bonding properties of liquid water from first principles. *J. Chem. Phys.* **111**, 3572.

Patel A., Price G. D. and Mendelssohn M. J. (1991) A computational simulation approach to modelling the structure, thermodynamics and oxygen isotope equilibria of silicates. *Phys. Chem. Min.* **17**, 690–699.

Pearce C. R., Saldi G. D., Schott J. and Oelkers E. H. (2012) Isotopic fractionation during congruent dissolution, precipitation and at equilibrium: evidence from Mg isotopes. *Geochim. Cosmochim. Acta* **92**, 170–183.

Perdew J. P., Burke K. and Ernzerhof M. (1996) Generalized gradient approximation made simple. *Phys. Rev. Lett.* **77**, 3685–3868.

Pinilla C., Irani A., Seriani N. and Scandolo S. (2012) Ab-initio parametrization of a fully polarizable and dissociable force field for water. *J. Chem. Phys.* **136**, 114511.

Pinilla C., Blanchard M., Balan E., Ferlat G., Vuilleumier R. and Mauri F. (2014) Equilibrium isotope fractionation of H and O isotopes in water from path integral molecular dynamics. *Geochim. Cosmochim. Acta*.

Polyakov V. B. and Mineev S. D. (2000) The use of Mössbauer spectroscopy in stable isotope geochemistry. *Geochim. Cosmochim. Acta* **64**, 849–865.

Ramirez R. and Herrero C. P. (2011) Kinetic energy of protons in ice Ih and water: a path integral study. *Phys. Rev. B* **84**, 064130.

Richet P., Bottinga Y. and Javoy M. (1977) A review of hydrogen, carbon, nitrogen, oxygen, sulphur, and chlorine stable isotope fractionation among gaseous molecules. *Ann. Rev. Earth Planet Sci.* **5**, 65–110.

Ross N. L. (1997) The equation of state and high-pressure behaviour of magnesite. *Am. Miner.* **82**, 682–688.

Ross N. L. and Reeder R. J. (1992) High-pressure structural study of dolomite and ankerite. *Am. Miner.* **77**, 412–421.

Rustad J. R. and Bylaska E. J. (2007) Ab-initio calculation of isotopic fractionation in $B(OH)_3$ (aq). *Geochim. Cosmochim. Acta* **129**, 2222.

Rustad J. R., Bylaska E. J., Jackson V. E. and Dixon D. A. (2010a) Calculation of boron-isotope fractionation between $B(OH)_3$(aq) and $B(OH)_4^-$(aq). *Geochim. Cosmochim. Acta* **74**, 2843–2850.

Rustad J. R., Casey W. H., Yin Q.-Z., Bylaska E. J., Felmy A. R., Bogatko S. A., Jackson V. E. and Dixon D. A. (2010b) Isotopic fractionation of Mg^{2+}, Ca^{2+}, and Fe^{2+} with carbonate minerals. *Geochim. Cosmochim. Acta* **74**, 6301–6323.

Saenger C. and Wang Z. (2014) Magnesium isotope fractionation in biogenic and abiogenic carbonates: implications for paleoenvironments proxies. *Quater. Sci. Rev.* **90**, 1–21.

Saulnier S., Rollion-Bard C., Vigier N. and Chaussidon M. (2012) Mg isotope fractionation during calcite precipitation: an experimental study. *Geochim. Cosmochim. Acta* **91**, 75–91.

Schauble E. A. (2011) First-principles estimates of equilibrium magnesium isotope fractionation in silicate, oxide, carbonate and hexaaquamagnesium(2^+) crystals. *Geochim. Cosmochim. Acta* **75**, 844–869.

Schauble E. A., Ghosh P. and Eiler J. M. (2006) Preferential formation of ^{13}C–^{18}O bonds in carbonate minerals, estimated using first-principles lattice dynamics. *Geochim. Cosmochim. Acta* **70**, 2170–2189.

Sherman D. M. (2013) Equilibrium isotopic fractionation of copper during oxidation/reduction, aqueous complexation and ore-forming processes: predictions from hybrid density functional theory. *Geochim. Cosmochim. Acta* **118**, 85–97.

Sit P. H.-L. and Marzari N. (2005) Static and dynamical properties of heavy water at ambient conditions from first-principles molecular dynamics. *J. Chem. Phys.* **122**, 204510.

Sprik M., Hutter J. and Parrinello M. (1996) Ab-initio molecular dynamics simulation of liquid water: comparison of three gradient-corrected density functionals. *J. Chem. Phys.* **105**, 1142.

Tazi S., Molina J. J., Rotenberg B., Turq P., Vuilleumier R. and Salanne M. (2012) A transferable ab-initio based force field for aqueous ions. *J. Chem. Phys.* **136**, 114507.

Togo A., Oba F. and Tanaka I. (2008) First-principles calculations of the ferroelastic transition between rutile-type and $CaC1_2$-type SiO_2 at high pressure. *Phys. Rev. B* **78**, 134106.

Tomasi J., Mennucci B. and Cammi R. (2005) Quantum mechanical continuum solvation models. *Chem. Rev.* **105**, 2999–3093.

Tuckerman M. E. and Berne B. J. (1993) Vibrational relaxation in simple fluids – comparison of theory and simulation. *J. Chem. Phys.* **98**, 7301.

Tuckerman M. (2010) *Statistical Mechanics: Theory and Molecular Simulation*. Oxford University Press.

de Villiers J. P. R. (1971) Crystal structures of aragonite, strontianite, and witherite. *Am. Mineral.* **56**, 758–767.

Wagner W. and Pruss A. (2002) Thermodynamic properties of ordinary water. *J. Chem. Ref. Data* **31**, 387–535.

Wang Z., Hu P., Gaetani G., Liu C., Saenger C., Cohen A. and Hart S. (2013) Experimental calibration of Mg isotope fractionation between aragonite and sea water. *Geochim. Cosmochim. Acta* **102**, 113–123.

Wilson E. B., Decius J. C. and Cross P. C. (1955) *Molecular Vibrations*. McGraw-Hill.

Wu L. L., Percak-Dennett E. M., Beard B. L., Roden E. E. and Johnson C. M. (2012) Stable iron isotope fractionation between aqueous Fe(II) and model Archean ocean Fe–Si coprecipitates and implications for iron isotope variations in the ancient rock record. *Geochim. Cosmochim. Acta* **84**, 14–28.

Yujie W., Tepper H. and Voth A. G. (2006) Flexible simple point-charge water model with improved liquid-state properties. *J. Chem. Phys.* **124**, 024503.

Associate editor: Andrew D. Jacobson